Food Chemistry: X 21 (2024) 101122

Contents lists available at ScienceDirect

Food Chemistry: X

journal homepage: www.sciencedirect.com/journal/food-chemistry-x

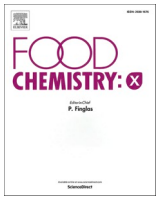

Recovery of soy whey protein from soy whey wastewater at various cavitation jet pretreatment time and their structural and emulsifying properties

Caihua Liu [a,b], Fuwei Sun [b], Yachao Tian [c], Lianzhou Jiang [b], Zhongjiang Wang [b,*], Linyi Zhou [a,*]

[a] College of Food and Health, Beijing Technology and Business University, Beijing 100048, China
[b] College of Food Science, Northeast Agricultural University, Harbin, Heilongjiang 150030, China
[c] School of Food Science and Engineering, Qilu University of Technology, Jinan, Shandong 250353, China

ARTICLE INFO

Keywords:
Cavitation jet
Soybean whey protein
Polysaccharide
Recovery yield
Emulsifying activity

ABSTRACT

Protein-polysaccharide composite is of great significance for the development of soluble protein recovery process. This study investigated the effects of cavitation jet (CJ) pretreatment at different time (0, 60, 120, 180, 240, 300 s) intervals on the recovery of soy whey protein (SWP) from soy whey wastewater using chitosan (CH). In addition, the structure and properties of the SWP/CH complexes were examined. The results showed that the recovery yield of SWP reached 84.44 % when the CJ pretreatment time was 180 s, and the EAI and ESI values of the SWP/CH complex increased from 32.39 m^2/g and 21 min to 48.47 m^2/g and 32 min, respectively. In the CJ pretreatment process, SWP promotes the recombination with chitosan through electrostatic interaction and hydrogen bond, while hydrophobic interaction is also involved. This study has guiding significance for CJ technology in the recovery and utilization of protein in industrial wastewater.

1. Introduction

Owing to its exceptional functional characteristics and low cost, soy protein isolate (SPI) has emerged as the most widely consumed plant-based protein worldwide. The production of every ton of SPI generates 20 t of soy whey wastewater (Wang, Wu, Zhao, Liu, & Gao, 2013). Untreated disposal of the majority of soy whey wastewater after production may lead to environmental pollution and significant depletion of valuable compounds such as soy whey protein (SWP) (Liu, Zhang, Wu, Wang, & Wang, 2013). SWP, a protein that can dissolve in acid and has significant nutritional benefits, can be added to different food products as a functional compounds owing to its high nutritional value (Tu et al., 2019). Additionally, SWP can serve as a structural agent or delivery system for bioactive substances in food, following chemical and physical alterations (Lavelli & Beccalli, 2022). Hence, the effective reuse of soy whey wastewater is anticipated to partially offset handling and disposal expenses while also generating valuable protein resources.

The conventional technique of using ammonium sulfate for precipitation can be employed to isolate SWP from soy whey wastewater. Salt precipitation for recovering proteins from wastewater is limited because of the need for strict control of salt concentration, easy decomposition of ammonium salts, and desalination of the product. The use of polysaccharides for flocculation and protein recovery is a distinct technique that has been extensively used for protein separation. Protein wastewater can be treated with chitosan due to its unique macromolecular composition and physicochemical properties. According the study of Wibowo et al. (2005), chitosan is an effective bioflocculant for the extraction of soluble proteins from surimi wash water. Enhancing the protein recovery efficiency in industrial-scale protein extraction processes can be achieved by incorporating physical field mediation. Nguyen et al. (2020) proposed a combination of ultrasonic extraction and chitosan co-precipitation as a highly effective method for extracting nutritional proteins from the heads of Australian Rock Lobsters. The results of studies have shown that the spatial conformational changes of proteins, including structural expansion and increased exposure of hydrophobic regions, will affect the recovery efficiency of polysaccharides. These changes may influence the processing and application of the resulting protein complex. According to a previous study conducted by Guo et al. (2023), CJ pretreatment has the potential to disrupt disulfide bonds within proteins, leading to the expansion of skeleton structures, reduction in aggregate sizes and molecular weights, and enhancement of emulsion activities. According to this study, the physical field produced

* Corresponding authors.
E-mail addresses: wzjname@126.com (Z. Wang), dorisneau@126.com (L. Zhou).

https://doi.org/10.1016/j.fochx.2024.101122
Received 6 December 2023; Received in revised form 24 December 2023; Accepted 4 January 2024
Available online 9 January 2024

by the CJ can boost the recuperation of SWP when treating soy whey water with polysaccharides and can also enhance the functional properties of the resulting complex by adjusting the spatial conformation of the SWP.

To test this hypothesis, the effect of chitosan on the recovery rate of soy whey protein and the structural properties and the emulsifying capability of SWP/CH complexes treated was investigated at different CJ pretreatment time (0, 60, 120, 180, 240, 300 s). This study developed a novel method on SWP recovery by CJ pretreatment assisted chitosan and provided theoretical support and reference significance for the recovery and reuse of food wastewater resources using CJ technology.

2. Materials and methods

2.1. Materials

Soy whey wastewater (solid content 2.2 ± 0.2 %, crude protein content (dry basis) 18 ± 0.5 %, pH 4.6 ± 0.1) was obtained from Shandong Yuwang Ecological Food Industry Co., Ltd. (Shandong, China). Chitosan (with a deacetylation degree of at least 85 %, 100,000 Da) was purchased from Shanghai Macklin Biochemical Technology Co., Ltd. (Shanghai, China). Corn oil was provided from Jiusan OILS and Grains Industries Group Co., Ltd. (Harbin, China).

Nile red, bicinchoninic acid assay (BCA) protein kit and sodium dodecyl sulfate (SDS) were bought from Yuanye Biotechnology Co. Ltd. (Shanghai, China). All other reagents used were analytical grade.

2.2. Formulation of samples for CJ pretreatment

The soy whey wastewater was rested at 4 °C for 24 h. Wastewater was centrifuged (8000 g, 30 min) to remove residual soy protein isolate. Adjust the pH of the supernatant to 8.0 and repeat the centrifugation step to obtain the supernatant. Dialysis (MW 3500 Da) the supernatant at 4 °C for 48 h to remove salt ions, the deionized water was replaced every 6 h. Then the protein concentration was diluted to 1 % (w/v). The soy whey wastewater was treated at 90 Mpa for 0, 60, 120, 180, 240, and 300 s by SL-2 Cavitation Jet Machine (Beijing Zhongsen Huijia Technology Development Co., LTD., China).

2.3. Recovery of SWP/CH complexes

The pH of soy whey wastewater with different CJ pretreatment time was adjusted to 6.0. Chitosan (1 % w/v) was added into soy whey wastewater at a ratio of 1:5 (chitosan:SWP). After stirring for 30 min, the solution rested for 4 h. The solution was centrifuged at 4 °C, 8000 g for 30 min to obtain the SWP/CH complexes precipitate. The SWP/CH complexes precipitate was dissolved in purified water and adjusted pH to 9.0. Let it sat overnight to remove insoluble chitosan. The solution was centrifuged for 30 min (8000 g, 4 °C) to obtain the supernatant. After adjusting the pH to 7.0, the solution was centrifuged for 30 min (8000 g, 4 °C) obtain the supernatant. Dialyze (MW 3500 Da) the supernatant for 48 h at 4 °C. During this process, the deionized water was replaced every 6 h. Then SWP/CH complexes were obtained by freeze-dried. These samples were named CJ-0, CJ-60, CJ-120, CJ-180, CJ-240, and CJ-300.

Control group was prepared following the modified techniques described by Sorgentini and Wagner (1999). Briefly, the proteins were through salting out using ammonium sulfate (75 %) at 25 °C and centrifuged for 30 min (8000 g, 4 °C) to obtain protein precipitate. Dissolved the protein precipitation in deionized water, then adjusted pH to 7.0 with HCl (2 mol/L). The dialysis and freeze-drying are the same as above. Samples was named Control. A flux diagram of sample preparation is shown in Fig. 1.

2.4. Recovery yield

The Kjeldahl method was employed to evaluate protein levels, which were then analyzed by the Kjeldahl system from Velp Scientifica (UDK 132, Italy). The results are expressed as the percentage of protein content, assuming a conversion factor of 6.25. Protein recovery was assessed using the method described by Jiang et al. (2022). Protein recovery yields were calculated as follows:

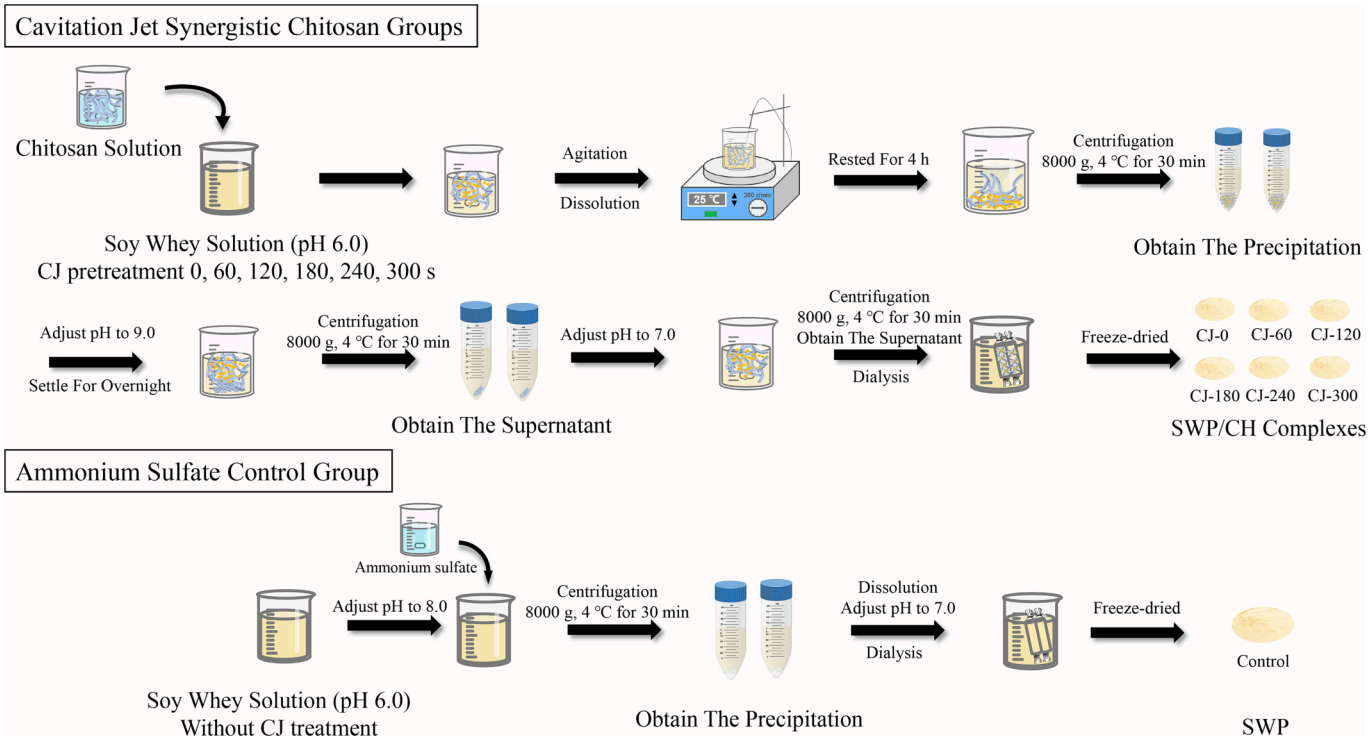

Fig 1. The preparation procedure of the Control, CJ-0, CJ-60, CJ-120, CJ-180, CJ-240 and CJ-300.

$$protein\ recovery\ yield\ (\%) = \frac{C_r \times W_r}{C_e \times V_e} \times 100\% \quad (1)$$

where C_r was the protein content of the SWP, W_r was the weight of the SWP after lyophilization, C_e was the protein content of soy whey wastewater and V_e was the volume of soy whey wastewater.

2.5. Isothermal titration calorimetry (ITC)

The method for measuring Isothermal titration calorimetry (ITC) was modified by Zhang et al. (2020). The thermodynamic properties and factors of complex coacervation between SWP and chitosan were determined at pH 6.0 and 25 °C using ITC-200 Microcalorimeter (Micro Cal Inc., Northampton, UK). At first, SWP solution (0.06 % w/v) and chitosan solution (0.12 % w/v) were degassing at 23 °C using a Micro Cal degasser. Afterwards, 1.7 mL SWP solution was added to the reaction cell, while the syringe contained 300 μL of chitosan solution. The dilution temperature was determined by titrating the chitosan solution with Milli-Q water under the same conditions and at the corresponding pH levels. Three measurements were obtained for each task.

2.6. Zeta potential

The deionized water as a solvent, samples were dissolved (0.1 % w/v). The zeta potential of each sample was measured using Malvern zeta potential analyzer (Malvern Pana Technology Co., Ltd., China), with a cuvette length of 1 cm^{-1} and a spacing of 0.4 cm^{-1}.

2.7. Particle size distribution and turbidity

A particle size analyzer (Nano-ZS90, Malvern Instruments, UK) was used to estimate the particle size distribution of the samples. To avoid multiple scattering effects, phosphate buffered saline (1 % w/v PBS, pH 7.0) was added to prepare diluted samples (0.1 % w/v). The refractive index was determined as 1.460, which was adjusted to 1.330 to account for the dispersant. Additionally, information on the polydispersity index (PDI) is provided. The measurements were conducted three times at 25 °C.

The absorbance at 600 nm was recorded using a UV–Visible spectrophotometer (UV-3900, Shimadzu, Japan) to measure the turbidity of samples. A blank reference was prepared using deionized water. The measurements were conducted three times at 25 °C.

2.8. Fourier transform infrared spectroscopy (FTIR) spectroscopy

The samples powder was pressed into tablets with KBr, the FTIR spectra was recorded using a IS10 FTIR spectrometer (Nicolet, US) in the wavenumber range 4000–400 cm^{-1}. The background for each test consisted of 32 air scans. The data was analyzed using Win GX (version 4.1) software. Spectra were baseline corrected and the first derivative spectra were plotted. Spectra were visually checked to ensure accuracy.

2.9. Surface hydrophobicity

Dilute the sample to a protein concentration of 0.1–1.0 % (w/v) by phosphate buffered saline (PBS, 1 % w/v, pH 7.0). Next, 20 μL of ANS were added to 4 mL of the prepared solutions. The intensity of the fluorescent signal was measured using Ultraviolet visible spectrophotometer (UV-3900, Shimadzu, Japan) at 390 nm and 465 nm (excitation and emission). The S_0 was acquired from gradient of the correlation between the fluorescence intensity and protein concentration (Xie et al., 2023).

2.10. Protein solubility

The method for measuring protein solubility was modified by Chen et al. (2023). Briefly, the sample solution (0.2 % w/v) was stirred for 15 min at 25 °C and centrifuged for 15 min (8000 g, 4 °C). The BCA protein kit was employed to determine the protein solubility in the supernatant. Using bovine serum protein as a standard.

2.11. Emulsifying activity index (EAI) and emulsion stability index (ESI)

The method for measuring EAI and ESI was modified by Li et al. (2020). In order to obtain the emulsion, 90 mL of solution (0.2 % w/v proteins) and 10 mL of corn oil were mixed and homogenized for three cycles using Spch-10 High-Pressure Homogenizer (AXA United Technology Co., Ltd. China) under 30 MPa. At 0 min and 20 min after homogenization, 50 μL of emulsion was immediately taken out at the bottom of the emulsion, and then diluted 100 times with SDS solution (1 % w/v). A spectrophotometer (Beckman DU 500, Fullerton, CA, USA) was used to determine absorbance at 500 nm. The EAI and ESI are defined as follows:

$$EAI\left(\frac{m^2}{g}\right) = \frac{2.302 \times 2 \times DF \times A_0}{10000 \times c \times \varepsilon \times (1-\theta)} \quad (2)$$

$$ESI\ (min) = \frac{A_0}{A_0 - A_{20}} \times (T_{20} - T_0) \quad (3)$$

where DF was the dilution factor multiplied by 100, A_0 was the absorbance of the thinned emulsion at 0 min, c was the protein concentration in grams per milliliter. ε was the optical path of 1 cm, θ was the volume fraction of the SWP/CH complex, which is 0.90, A_{20} was the absorbance after 20 min, T_{20} was a duration of 20 min, T_0 was a duration of 0 min.

2.12. Confocal laser scanning microscope (CLSM)

For sample staining, 500 μL of newly prepared emulsions were darkly stained with a mixture of 20 μL fluorescent dye composed of Nile red and Nile blue (0.1 % w/v, dissolved by absolute isopropanol). Nile Red was excited at 488 nm, whereas Nile Blue was excited at 633 nm (Ki, Parameswaran, Popat, Rittmann, & Torres, 2015).

2.13. Adsorbed protein percentage (AP%)

The method for measuring adsorbed protein percentage was modified by Liang and Tang (2013). The samples emulsion was centrifuged for 15 min (8000 g, 20 °C) to obtain an upper layer, called the emulsion layer, and a lower layer, known as the aqueous phase. The lower aqueous phase was extracted using a syringe and filtered through a 0.22 μm membrane to determine the protein content in the aqueous phase using the BCA method. The adsorbed protein percentage (AP %) was calculated as follows,

$$AP\ (\%) = \frac{C_0 - C_S}{C_0} \times 100\% \quad (4)$$

where C_0 was the protein concentration in the initial protein solution, C_S was the concentration of the protein that has not been adsorbed.

2.14. Statistical analysis

Statistical analyses were performed using SPSS version 26.0. Measurements were conducted in triplicate which is independent. The outcomes were reported as the average plus the standard deviation (SD). Duncan multiple comparison method was used to conduct one-way ANOVA on the data, and the significance was set at $p < 0.05$.

3. Results and discussion

3.1. Recovery yield

SWP recovery in Control and CJ pretreatment synergistic chitosan groups is shown in Fig. 2 A. The process of extracting SWP using ammonium sulfate involves the utilization of NH_4^+ and SO_4^{2-} ions to precipitate SWP, which disrupts surface hydration. SWP was recovered through the salting-out effect. Chitosan offers a polycationic property that serves as an ionizable polyelectrolyte in solution, which has the ability to enhance the flocculation of SWP through electrostatic interactions (Nguyen, Luo, Su, Balakrishnan, & Zhang, 2020), allowing SWP to be recovered. The result showed that the recovery rate of SWP using chitosan was higher than the Control. Therefore, the recovery of SWP using chitosan is advantageous for protein recovery in food processing streams. However, the spatial structural variation of SWP can directly affect their recovery by chitosan through electrostatic interactions. The structure of SWP was altered by CJ pretreatment, and the effect of chitosan on the recovery of SWP at different pretreatment times was evaluated. With an increase in the CJ pretreatment time, the recovery rate of SWP using chitosan showed a trend of first increased and then decreased. The flexibility and overall charge of the SWP molecules are increased by mechanical shear, thermal decomposition, and free radical oxidation effects induced by the CJ (Guo et al., 2023). This improved the flocculation of SWP by exposing more binding sites for electrostatic interactions with chitosan. However, the extended duration of CJ pretreatment elicits the re-aggregation of SWP, impedes its unfolding, and diminishes the availability of binding sites on the SWP surface for chitosan. Therefore, the decrease in the binding ability between aggregated SWP and chitosan leads to a decrease in the recovery rate of SWP.

3.2. ITC

ITC is a direct method for examining the interactions between SWP and chitosan (Campiña et al., 2010). Fig. 3 showed the CJ-0 and CJ-180 samples produced heat flow over time. The heat flow was negative, suggesting that the interaction between the SWP and chitosan was exothermic. Dong et al. (2015) have reported similar results. The SWP isotherm for chitosan titration showed high exothermic peaks at the beginning, followed by a constant decrease in temperature over time. Because coacervation between SWP and chitosan was primarily driven by negative enthalpy caused by electrostatic interactions. The observed increase in the number of chitosan injections required to achieve saturation during the titration of SWP confirming that the duration of CJ pretreatment enhances the electrostatic attraction between SWP and chitosan. Table 1 displays thermodynamic parameters. These parameters provided additional support for enthalpically favorable and entropically unfavorable interactions between SWP and chitosan during the SWP/CH complexation process. The parameters of ΔH also indicate that the complexation of SWP and chitosan has a strong driving force. Furthermore, the complexation process is exothermic.

The K_D values of the CJ-0 and CJ-180 groups were below 10^{-6}. This indicates the significant strength of the interactions between the two polymers, because the complexes are deemed to possess a high affinity while K_D values were below 10^{-6}(Franca, Lins, Freitas, & Straatsma, 2008). A negative ΔG value indicates that the interactions between SWP and chitosan were consistently spontaneous, suggesting that the interaction between SWP and chitosan follows the pattern of associative phase separation (Rabelo, Tavares, Prata, & Hubinger, 2019). In the

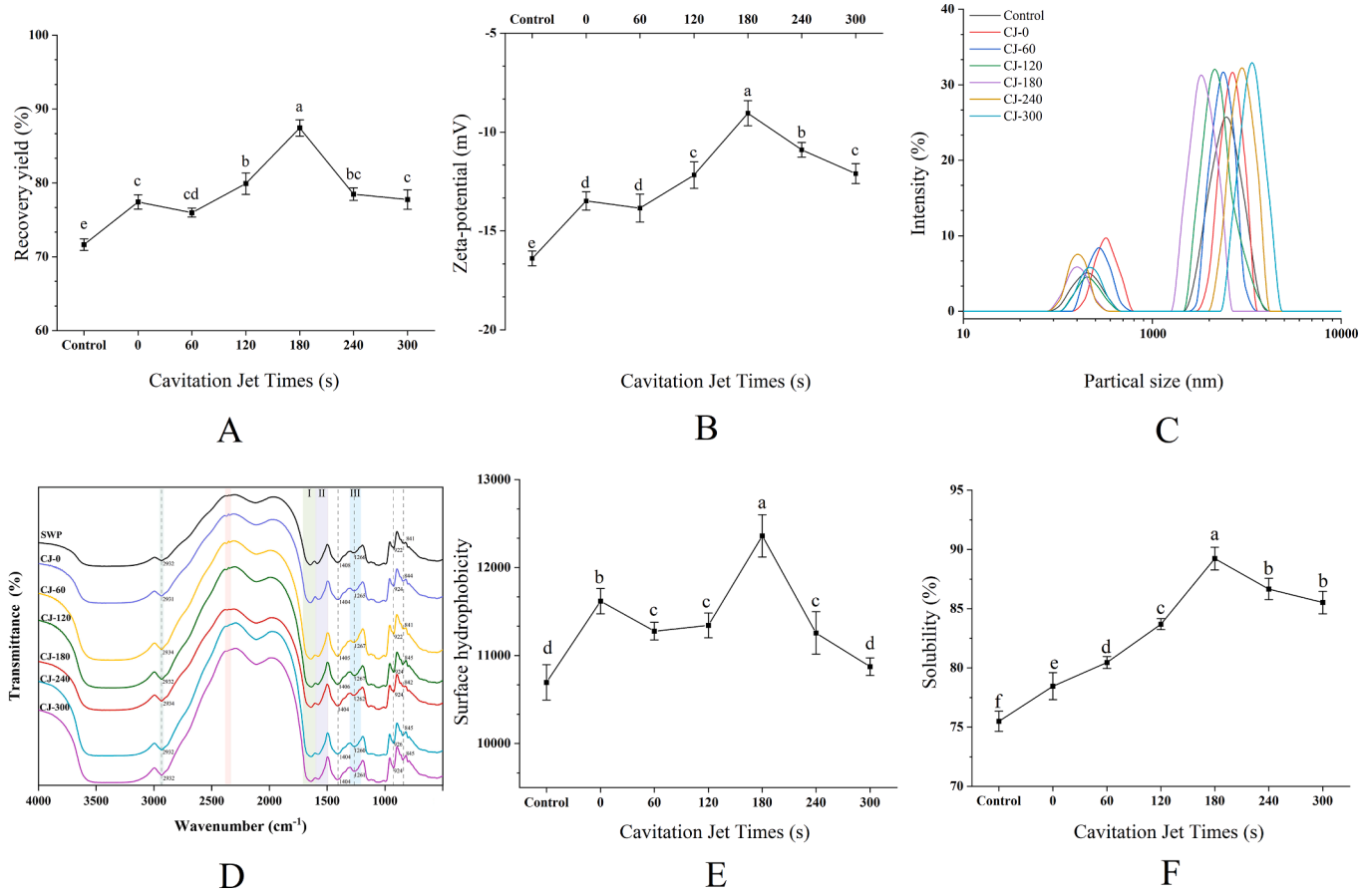

Fig 2. Recovery yield (A), Zeta-potential (B), Particle size (C), Fourier transform infrared spectrum (D), Surface hydrophobicity (E), Solubility (F) of the Control, CJ-0, CJ-60, CJ-120, CJ-180, CJ-240 and CJ-300. Different lowercase letters mean significant differences at $p < 0.05$ between different samples.

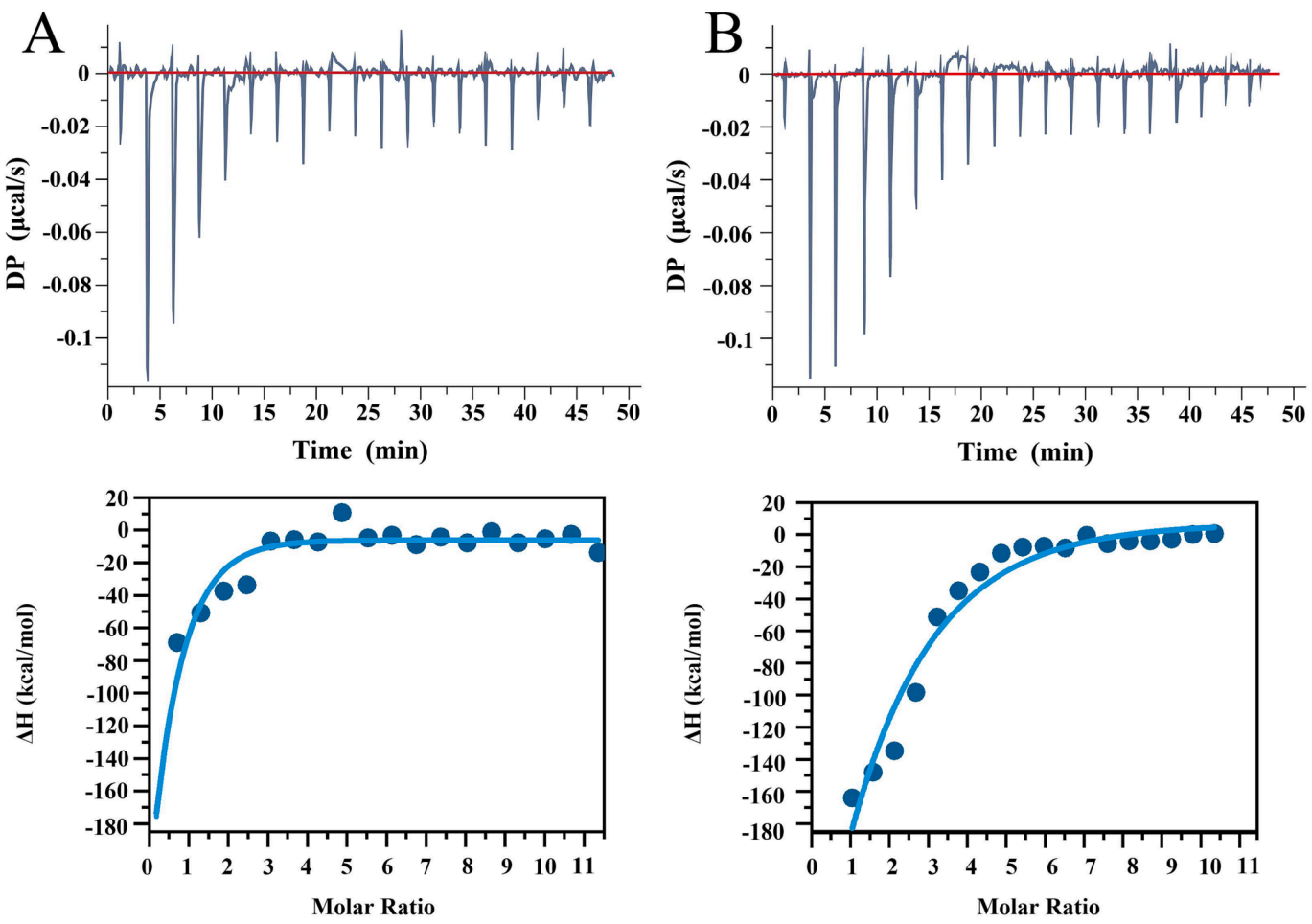

Fig 3. Thermograms (top panels) and binding isotherms (bottom panels) corresponding to the titration of the soy whey protein (SWP) solution with chitosan solution. Soy whey protein (SWP) was obtained from freeze-dried soy whey wastewater without cavitation jet pre-treatment (A) and freeze-dried soy whey wastewater after cavitation jet pre-treatment for 180 s (B), respectively.

Table 1
Thermodynamic parameters of binding between soy whey protein (SWP was obtained by freeze-dried soy whey wastewater without cavitation jet pretreatment which is named CJ-0 and freeze-dried soy whey wastewater after cavitation jet pre-treatment for 180 s which is named CJ-180, respectively) and chitosan (CH).

Samples	N	K_D (M)	ΔG (kcal/mol)	ΔH (kcal/mol)	-TΔS (kcal/mol)
CJ-0	3.40×10^{-3}	731×10^{-9}	−8.37	−56.60	48.23
CJ-180	4.71×10^{-3}	852×10^{-9}	-11.95	-63.64	51.69

complex coacervation between SWP and chitosan at various CJ pretreatment durations (0 and 180 s), an electrostatic interaction between the two oppositely charged components produced most of the negative enthalpy (negative contribution to ΔG) (Vuillemin, Michaux, Muniglia, Linder, & Jasniewski, 2019). The formation of SWP and chitosan complex involves electrostatic interactions that occur at a larger distance than hydrogen bonds and van der Waals interactions (Grinberg & Tolstoguzov, 1997). The denaturation of SWP induced by CJ pretreatment enables it to adapt to the charge density of chitosan by facilitating the formation of electrostatic complexes, which is accompanied by merging, fusion, or recombination of the complexes. This increased the enthalpy of the reaction system. Furthermore, the CJ pretreatment led to a positive alteration in entropy and an enhancement in affinity. The presence of non-electrostatic interactions was manifested by a stronger binding affinity between SWP and chitosan, leading to a reduction in entropy (Bolel, Datta, Mahapatra, & Halder, 2012). Indeed, the CJ pretreatment enhances hydrophobic interactions by causing conformational changes in the SWP structure and releasing bound water and counterions into the bulk (Mu et al., 2022). The formation of hydrogen bonds was facilitated by the presence of glutamate as the SWP molecules were pulled together by electrostatic interactions. In contrast, with a CJ pretreatment time of 180 s, the stabilizing intermolecular interactions in the SWP/CH system were substituted by cooperative interactions between protein molecules along the chitosan chain. This change occurred because of the disruption of the hydrogen bonding. The inclusion of all charges in the interactions of the SWP/CH complexes led to a decrease in randomness and an increase in the order within the system (Du, Hong, Cheng, & Gu, 2022). In addition, during the 180 s CJ pretreatment, the ions from the SWP acted as a protective barrier and reduced the impact of electrostatic interactions on the charge of the polyelectrolytes in the solution. The combination of SWP and chitosan exhibited a beneficial change in enthalpy ($\Delta H < 0$), which is partly counteracted by an unfavorable change in entropy ($\Delta S < 0$). This compensation was linked to the equilibrium of SWP/CH electrostatic and hydrophobic interactions, which play a pivotal role in the creation and maintenance of complex.

3.3. Zeta potential

The zeta potential reflects the intensity of electrostatic repulsion or attraction particle surface of the SWP/CH complexes (Li, Xu, & Xu,

2022). Therefore, the zeta potentials of the control and CJ-pretreated synergistic chitosan groups were determined. As shown in Fig. 2 B, the absolute value of the zeta potential in the CJ-0 group was lower than that of the Control. This may be because the positively charged chitosan interacted with the negatively charged SWP via electrostatic interactions, and the binding strength between chitosan and SWP was higher than that of ammonium sulfate, thus causing the zeta potential of CJ-0 to be lower than that of the Control. The absolute value of the zeta potential of the SWP/CH complexes first decreased and then increased with increasing pretreatment time of CJ. When the pretreatment time of CJ was 180 s, the zeta potential reached its minimum value. This might be because an appropriate CJ pretreatment can break the skeleton structures of SWP and increase the flexible molecular structure and surface area of SWP, thus exposing more charged groups and facilitating the possibility of binding to SWP (Cheng et al., 2024). This change could cause the negative charge on the SWP surface to be neutralized by the greater positive charge on the chitosan surface, thereby reducing the absolute zeta potential of the SWP/CH complexes. This was also confirmed from another perspective: chitosan enhanced the recovery rate of SWP through electrostatic interactions, which were related to the pretreatment time of CJ. The results is agreed with those of previous studies (Mounsey, O'Kennedy, Fenelon, & Brodkorb, 2008). When the pretreatment time of CJ is prolonged, cavitation and thermal effects can lead to the dissociation and aggregation of SWP, thereby destroying some of the chitosan binding sites. This can lead to a decrease in the number of positively charged chitosan molecules bound to SWP and retention of exposed negatively charged amino acid residues, resulting in an increase in the absolute value of the zeta potential of SWP/CH complexes.

3.4. Particle size distribution and turbidity

The particle size distribution and turbidity of the control and CJ-pretreated chitosan groups are shown in Fig. 2 C and Table 2. The particle size and turbidity of the CJ group were higher than those of the Control due to the flocculation of SWP and chitosan. High turbidity indicates strong cohesion between SWP and chitosan (Amine, Boire, Kermarrec, & Renard, 2019). The particle size and turbidity of the SWP/CH complexes first decreased and then increased with increasing CJ pretreatment time, with the CJ-180 group exhibiting the smallest particle size and turbidity. This is because the cavitation cleavage effect produced by the appropriate CJ disperses SWP into small particles, which exposes more hydrophobic groups and can form small SWP/CH complexes via charge neutralization. Smaller SWP/CH complex were better dispersed in the water phase, thereby reducing the turbidity of the solution. However, the change in the spatial structure of small SWP particles caused by long-term cavitating jet pretreatment led to the reaggregation of the SWP. Strong hydrophobic and hydrogen bond interactions between the reaggregates of SWP led particle size increase and turbidity when combined with chitosan. The trend of PDI variation is similar to that of particle size variation, which may be because effective charge neutralization between SWP and CH is conducive to the formation of uniformly sized and distributed complexes (Zhang, Dong, Gao, Chen, & Vasanthan, 2020).

Table 2
Polymer dispersity index (PDI) and turbidity of the Control, CJ-0, CJ-60, CJ-120, CJ-180, CJ-240 and CJ-300.

Samples	PDI	Turbidity
Control	0.45 ± 0.02^{a}	0.24 ± 0.02^{ab}
CJ-0	0.47 ± 0.04^{a}	0.27 ± 0.01^{a}
CJ-60	0.43 ± 0.05^{ab}	0.22 ± 0.02^{b}
CJ-120	0.39 ± 0.01^{bc}	0.18 ± 0.01^{c}
CJ-180	0.37 ± 0.01^{c}	0.14 ± 0.02^{d}
CJ-240	0.38 ± 0.06^{bc}	0.18 ± 0.01^{c}
CJ-300	0.35 ± 0.02^{c}	0.19 ± 0.01^{c}

Note: Different lowercase letters in the same column mean significant differences at $p < 0.05$ between different samples.

3.5. FTIR

The stretching of chemical bonds and conformational changes in the SWP/CH complexes were assessed by FTIR. As shown in Fig. 2 D, the spectra were almost identical and the addition of polysaccharides did not cause new characteristic peaks to appear for CJ-0, indicating that the incorporation of chitosan did not induce additional covalent bonds in the SWP/CH complexes. The characteristic peaks at 1575–1480 cm^{-1} are mostly attributed to the C—O stretching and N—H bending of the amide bonds (Wang, Yang, Du, & Chen, 2023). The characteristic peak intensity of CJ-0 significantly increased at 1536 cm^{-1}, and the characteristic peak intensity changed with increasing CJ pretreatment time. The blue shift of the peak in the spectrum at about 2932 cm^{-1} and 842 cm^{-1} corresponds to the stretching vibration of $–CH_2$ and the deformation vibration of –CH. This is caused by the vibration of hydrogen bond interaction between SWP and chitosan (Mohammadian & Madadlou, 2016). The characteristic peaks of FTIR spectroscopy at 2962 cm^{-1} correspond to the stretching vibration of hydrophobic C—H. However, the shapes and intensities of the CJ-0 and CJ-60 to CJ-300 samples were altered to a certain degree, suggesting the existence of hydrophobic interactions within the SWP/CH complexes.

As shown in Table 3, chitosan and CJ pretreatment times significantly changed the composition of protein secondary structures in SWP. Compared with SWP, the β-turn and random coil content of the SWP/CH complexes decreased, and α-helix and β-sheet content increased. These results suggested that the noncovalent binding of SWP to chitosan promoted the conversion of β-turn regions and random coil regions to α-helix and β-sheet regions, and the increase in α-helix and β-sheet content also indicated that the structure of SWP/CH complex became more compact (Gao et al., 2013). Furthermore, with an increase in the CJ pretreatment time from 60 s to 300 s, the α-helix and β-sheet of the SWP/CH complexes first decreased and then increased, and the β-turn and random coil increased first and then decreased. When the CJ pretreatment time was 180 s, the α-helix content of SWP/CH complex was the lowest. In protein secondary structures, α-helices and β-sheets of proteins are considered ordered structures (Xue et al., 2022). The cavitation bubbles render the SWP structure looser and more stretched, and the ordered structures are converted into disordered structures (Guo et al., 2023). This structure promoted the interaction between SWP and chitosan, thus more chitosan molecules were bound. Furthermore, the excessive pretreatment time of CJ would cause the protein aggregation, thus increasing the α-helix and β-sheet content.

3.6. Surface hydrophobicity

Surface hydrophobicity measurements were conducted to assess alterations in the stability and conformation of the SWP/CH complexes (Zhan et al., 2019), which affect their functionality of SWP/CH

Table 3
Secondary structure content of the Control, CJ-0, CJ-60, CJ-120, CJ-180, CJ-240 and CJ-300.

Samples	Content (%)			
	α-helix	β-sheet	β-turn	random coil
Control	17.84 ± 0.03^{e}	30.05 ± 0.04^{a}	37.16 ± 0.09^{a}	14.95 ± 0.01^{e}
CJ-0	21.34 ± 0.09^{b}	29.55 ± 0.05^{b}	32.64 ± 0.09^{d}	16.48 ± 0.08^{c}
CJ-60	21.14 ± 0.07^{c}	29.32 ± 0.08^{c}	32.30 ± 0.04^{e}	17.24 ± 0.07^{b}
CJ-120	19.63 ± 0.04^{d}	29.69 ± 0.08^{b}	33.37 ± 0.07^{c}	17.31 ± 0.02^{b}
CJ-180	17.08 ± 0.03^{f}	28.87 ± 0.04^{d}	35.92 ± 0.04^{ab}	18.12 ± 0.04^{a}
CJ-240	21.58 ± 0.02^{a}	29.33 ± 0.03^{c}	36.14 ± 0.03^{a}	15.79 ± 0.05^{d}
CJ-300	19.62 ± 0.09^{d}	21.45 ± 0.06^{e}	34.16 ± 0.06^{b}	14.38 ± 0.04^{f}

Note: Different lowercase letters in the same column mean significant differences at $p < 0.05$ between different samples.

complexes. As shown in Fig. 2E, the surface hydrophobicity of the CJ-0 group was higher than that of the Control. This suggests that the tertiary structure of SWP undergoes changes in the presence of chitosan, thus changing the hydrophobic forces (Song, Zhong, Sun, Li, & Qi, 2023). The surface hydrophobicity of the SWP/CH complexes first increased and then decreased with increasing CJ pretreatment time, and the surface hydrophobicity of CJ-180 was the highest. This is because the high-pressure shear effect of the CJ weakens the intramolecular forces of SWP, which induces the unfolding of SWP and the extension of the noncovalent bonds of the SWP molecules, thereby exposing the hydrophobic groups buried in the SWP (Man et al., 2023). CJ pretreatment and the presence of chitosan together led to an increase in the surface hydrophobicity of the SWP/CH complexes. The surface hydrophobicity of the SWP/CH complexes decreased when the CJ pretreatment time exceeded 180 s. This may have been due to the cavitation and shear stress generated by excessive CJ, which caused intermolecular hydrophobic aggregation of SWP and a decrease in the amount of binding with chitosan, thus reducing the surface hydrophobicity of the SWP/CH complexes.

3.7. Protein solubility

Solubility characterizes the degree of protein denaturation and aggregation and affects many functional properties of proteins. As shown in Fig. 2 F, the solubility of the CJ-0 group was significantly higher than that of the Control. This is because the addition of CH and introduction of a large number of hydroxyl groups into the complex increased the solubility of the SWP/CH complexes. The solubility of the SWP/CH complexes first increased and then decreased with increasing CJ pretreatment time, with the highest solubility observed in CJ-180 s. The intense disruptive forces caused by CJ could effectively break down larger protein particles into smaller ones and increase the specific surface area to bind with more chitosan, which further enhanced the SWP/water and SWP/CH interactions, thus leading to increased solubility of the SWP/CH complexes (Sliwinski, Roubos, Zoet, van Boekel, & Wouters, 2003). However, prolonged CJ can cause protein molecules to expand, exposing hydrophobic groups. The SWP molecules formed macromolecular aggregates through noncovalent interactions, burying the binding sites with chitosan, which resulted in a decrease in the solubility of the SWP/CH complexes.

3.8. Emulsifying capacity

3.8.1. EAI and ESI

The emulsifying properties serve as metrics to assess the capacity of emulsifiers to stabilize emulsions at the O/W interface, as quantified by EAI and ESI. As shown in Fig. 4 A, the EAI and ESI of CJ-0 increased significantly compared with those of the Control because the interactions between SWP and chitosan could lead to the exposure of hydrophobic residues outside the protein molecule, which were

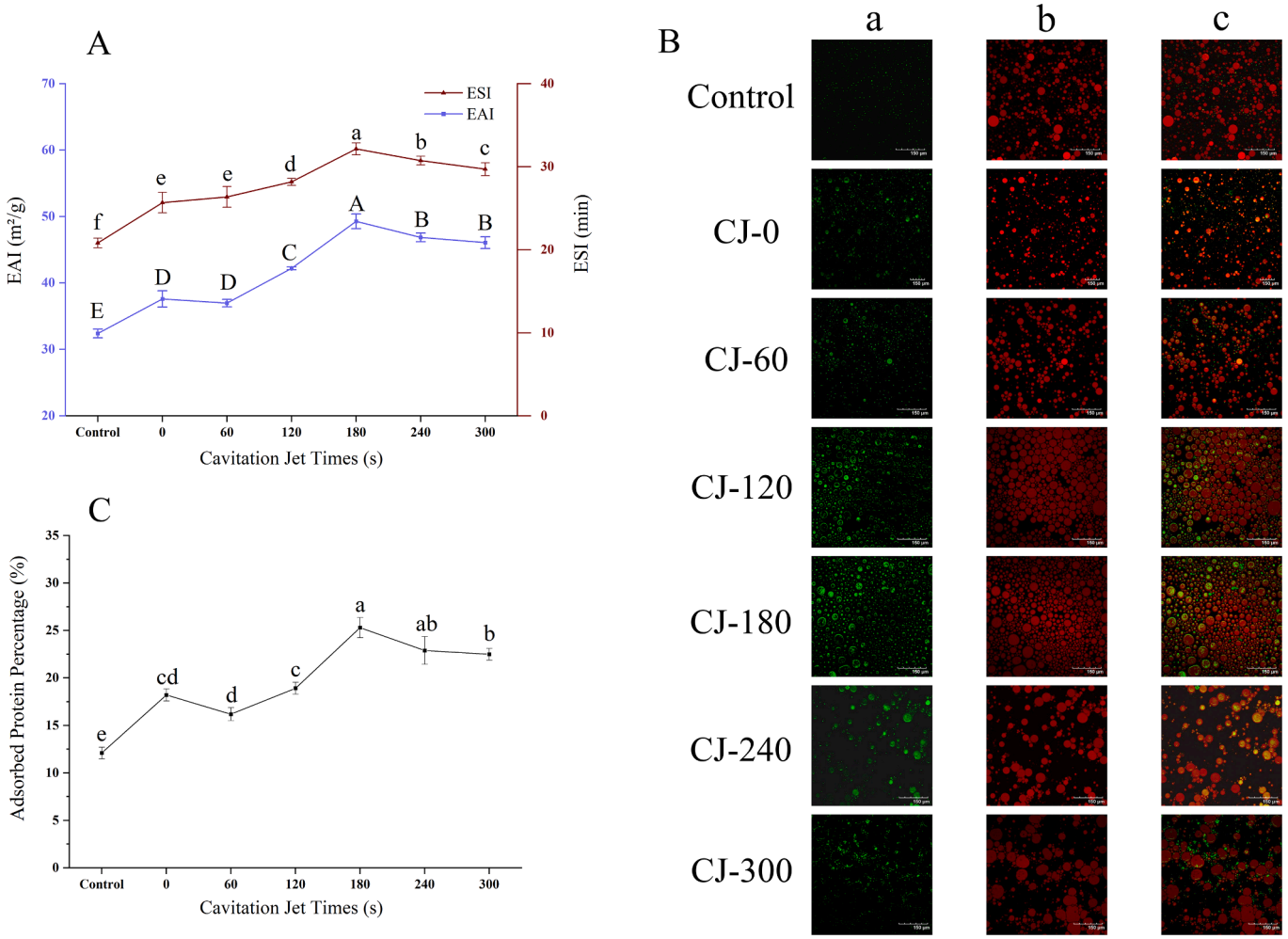

Fig 4. Emulsifying activity (EAI) and emulsifying stability (ESI) (A), Confocal laser scanning microscopy (CLSM, Scale bar = 150 μm) (B), Adsorbed protein percentage (AP %) (C) of the Control, CJ-0, CJ-60, CJ-120, CJ-180, CJ-240 and CJ-300. Different capital letters and lowercase letters mean significant differences at $p < 0.05$ between different samples.

absorbed onto the O/W interface, improving the stability of the emulsion (Wang et al., 2019). The EAI and ESI of the SWP/CH complexes exhibited an initial increase, followed by a decline as the pretreatment time of CJ increased, suggesting that appropriate pretreatment of CJ was favorable for forming an O/W emulsion. Appropriate pretreatment with CJ might increase the intermolecular electrostatic repulsion and hydrophobic interactions of SWP and accelerate the adsorption of chitosan onto SWP, thereby allowing SWP/CH complexes to adsorb and rearrange more quickly at the oil/water interface, ultimately enhancing EAI and ESI (Kato, 2002). However, the excessive pretreatment of CJ may lead to the decrease of EAI and ESI of SWP/CH complex, potentially attributed to the diminished surface hydrophobicity. The lower surface hydrophobicity increased the energy required for the SWP/CH complexes to adsorb onto the oil–water interface, hindering the adsorption of SWP/CH complexes and the formation of dense interfacial protein membranes (de Oliveira, Coimbra, de Oliveira, Zuñiga, & Rojas, 2016).

3.8.2. CLSM

The CLSM results for the emulsions prepared with SWP/CH complexes were shown in Fig. 4 B. The SWP/CH complexes were dyed green and formed a shell structure on the outside of the oil droplets, whereas the oil phase was dyed red and wrapped inside. Control (Fig. 4 B Control c) sample was observed that SWP was dispersed in the lotion phase, and only a small amount was adsorbed on the surface of oil droplets. The lotion drops are spherical with uneven size distribution. As the pretreatment time of CJ increased, the surface of oil droplets (Fig. 4 B CJ-60c, CJ-120c, CJ-180c) is enveloped by SWP/chitosan complexes due to their "shell" state (Fig. 4 B CJ-120 a, CJ-180 a). The appropriate CJ pretreatment could reduce the particle size of SWP and cause SWP to adsorb more chitosan to form smaller SWP/CH complexes. The presence of chitosan can produce an osmotic driving force, thereby reducing the interfacial tension and enhancing the amphiphilicity of the SWP/CH complexes. This helped it better adsorb at the oil–water interface and form a stable and thick protein adsorption layer to stabilize emulsion droplets of smaller particle sizes (Xie et al., 2023). After prolonged pretreatment with CJ, the droplets size increased accompanied with irregular spherical. The SWP/CH complexes with large particle sizes produced by the excessive pretreatment time of CJ had lower surface hydrophobicity, thereby inhibiting adsorption at the oil–water interface. In addition, SWP/CH complexes with large particle sizes exhibit relatively high vacancy resistance and electrostatic repulsion, making protein film formation difficult. Consequently, large aggregates of emulsion droplets are formed, causing emulsion instability. This is why it is important to consider the appropriate pretreatment time in order to reduce the particle size of the SWP/CH complexes.

3.8.3. Adsorbed protein percentage (AP%)

To better understand the interfacial properties of the emulsion, the adsorbed protein percentage (AP %) was measured and used as an indicator of interfacial protein adsorption capacity (Wang, Wang, Dai, Yu, & Cheng, 2023). The AP% of the control and SWP/CH complexes after different CJ pretreatment times are shown in Fig. 4 C. Compared with the control, the AP% of CJ-0 was significantly increased. This may be due to the formation of soluble complex between SWP and chitosan, which can increase the AP content at the interface (Huang et al., 2023). With increasing CJ pretreatment time, the AP% content showed an increasing trend, followed by a slight decrease. The AP% content was highest when the CJ pretreatment time was 180 s. This result proved that CJ pretreatment promoted the adsorption of SWP/CH complexes on the oil–water surface. CJ pretreatment reduced the particle size of SWP and promoted the binding of SWP with chitosan, which led to greater thermodynamic incompatibility between SWP and chitosan, thus promoting the diffusion and adsorption of the protein to the interface and making it easier to rearrange at the oil–water interface (Bergfreund, Bertsch, & Fischer, 2021). When the CJ pretreatment time was increased to 300 s, the AP% slightly decreased. Excessive pretreatment time of CJ could lead to the phenomenon of "overprocessing," and the formation of complex systems of larger particles and fewer hydrophobic groups would be unfavorable for adsorption of SWP/CH complexes. Simultaneously, the reduction in the hydrophobic point of the SWP/CH complex leads to a decrease in the intermolecular connections among proteins. This decrease in protein particle adhesion onto the oil–water surface consequently results in a reduction in the AP% value.

4. Conclusion

In this study, SWP was recovered by using CJ pretreatment combined with chitosan. The proper CJ pretreatment of soy whey wastewater is beneficial for the binding of chitosan and SWP, thereby the recovery rate of SWP increased. Afterwards, we analyzed the binding mechanisms and emulsifying capacity of SWP/CH complexes. The FTIR and ITC results indicated that SWP and chitosan mainly bind through non covalent interactions, with electrostatic interactions being the most important. In addition. The SWP/CH complexes obtained by proper CJ pretreatment had a smaller particle size distribution and higher surface hydrophobicity, which was conducive to their adsorption on the oil–water interface, thus stabilizing the emulsion. While CJ pretreatment time was 180 s, the ability of SWP/CH compound to stabilize emulsion reaches the maximum. However, the obtained results could be affected by the variability in the composition of raw material (soy whey wastewater) and chitosan commercial samples, which can exhibit different density charges and molecular weights. Therefore, it is necessary to further study the interaction mechanism between protein structure changes and polysaccharides with different density, charge and molecular weight, so as to better play the role of cavitating jet technology in the treatment of food industry wastewater.

Funding

This research was funded by the "14th Five-Year Plan" National Key R&D Program of China (2021YFD2100400), the Heilongjiang Province "Hundreds and Thousands" Engineering Science and Technology Major Project (2021ZX12B02), the Shandong Province Major R&D Project (2022CXGC010603).

CRediT authorship contribution statement

Caihua Liu: Writing – original draft, Conceptualization. **Fuwei Sun:** Visualization, Methodology, Data curation. **Yachao Tian:** Supervision, Investigation. **Lianzhou Jiang:** Resources, Software. **Zhongjiang Wang:** Supervision, Project administration. **Linyi Zhou:** Funding acquisition, Conceptualization.

Declaration of competing interest

The authors declare that they have no known competing financial interests or personal relationships that could have appeared to influence the work reported in this paper.

Data availability

Data will be made available on request.

References

Amine, C., Boire, A., Kermarrec, A., & Renard, D. (2019). Associative properties of rapeseed napin and pectin: competition between liquid-liquid and liquid-solid phase separation. *Food Hydrocolloids, 92*, 94–103. https://doi.org/10.1016/j.foodhyd.2019.01.026

Bergfreund, J., Bertsch, P., & Fischer, P. (2021). Adsorption of proteins to fluid interfaces: role of the hydrophobic subphase. *Journal of Colloid and Interface Science, 584*, 411–417. https://doi.org/10.1016/j.jcis.2020.09.118

Bolel, P., Datta, S., Mahapatra, N., & Halder, M. (2012). Spectroscopic investigation of the effect of salt on binding of tartrazine with two homologous serum albumins:

quantification by use of the debye–hückel limiting law and observation of enthalpy–entropy compensation. *The Journal of Physical Chemistry B, 116*(34), 10195–10204. https://doi.org/10.1021/jp304537m

Campiña, J. M., Souza, H. K. S., Borges, J., Martins, A., Gonçalves, M. P., & Silva, F. (2010). Studies on the interactions between bovine β-lactoglobulin and chitosan at the solid–liquid interface. *Electrochimica Acta, 55*(28), 8779–8790. https://doi.org/10.1016/j.electacta.2010.08.012

Chen, F., Lin, L., & Zhao, M. (2023). Co-extraction of soy protein and polysaccharide with lipid-lowering activity: characterization of functional property, nutritional property and colonic fermentation property through a metabolomics approach. *Food Hydrocolloids, 138*, Article 108472. https://doi.org/10.1016/j.foodhyd.2023.108472

Cheng, T., Wang, Z., Sun, F., Liu, H., Liu, J., Guo, Z., & Zhou, L. (2024). Gel properties of rice proteins-pectin composite and the delivery potential for curcumin: based on different concentrations and the degree of esterification of pectin. *Food Hydrocolloids, 146*, Article 109305. https://doi.org/10.1016/j.foodhyd.2023.109305

De Oliveira, F. C., Coimbra, J. S. D. R., De Oliveira, E. B., Zuñiga, A. D. G., & Rojas, E. E. G. (2016). Food protein-polysaccharide conjugates obtained via the maillard reaction: a review. *Critical Reviews in Food Science and Nutrition, 56*(7), 1108–1125. https://doi.org/10.1080/10408398.2012.755669

Dong, D., Li, X., Hua, Y., Chen, Y., Kong, X., Zhang, C., & Wang, Q. (2015). Mutual titration of soy proteins and gum arabic and the complexing behavior studied by isothermal titration calorimetry, turbidity and ternary phase boundaries. *Food Hydrocolloids, 46*, 28–36. https://doi.org/10.1016/j.foodhyd.2014.11.019

Du, J., Hong, Y., Cheng, L., & Gu, Z. (2022). Complexation behavior of carboxymethyl short-chain amylose and quaternized chitosan. *International Journal of Biological Macromolecules, 209*, 1914–1921. https://doi.org/10.1016/j.ijbiomac.2022.04.165

Franca, E. F., Lins, R. D., Freitas, L. C. G., & Straatsma, T. P. (2008). Characterization of chitin and chitosan molecular structure in aqueous solution. *Journal of Chemical Theory and Computation, 4*(12), 2141–2149. https://doi.org/10.1021/ct8002964

Gao, X., Sun, P., Lu, J., & Jin, Z. (2013). Characterization and formation mechanism of proteins in the secondary precipitate of soy sauce. *European Food Research and Technology, 237*(4), 647–654. https://doi.org/10.1007/s00217-013-2054-2

Grinberg, V. Y., & Tolstoguzov, V. B. (1997). Thermodynamic incompatibility of proteins and polysaccharides in solutions. *Food Hydrocolloids, 11*(2), 145–158. https://doi.org/10.1016/S0268-005X(97)80022-7

Guo, Y., Liu, C., Wang, Y., Ren, S., Zheng, X., Zhang, J., Cheng, T., Guo, Z., & Wang, Z. (2023). Impact of cavitation jet on the structural, emulsifying features and interfacial features of soluble soybean protein oxidized aggregates. *Foods, 12*(5), 909. https://doi.org/10.3390/foods12050909

Huang, M., Xu, Y., Xu, L., Bai, Y., Zeng, X., Zheng, R., & Xu, X. (2023). Conformation changes and emulsifying properties of myofibrillar proteins in water: Effects of electrostatic interaction with chitosan. *Food Research International, 163*, Article 112154. https://doi.org/10.1016/j.foodres.2022.112154

Jiang, Y., Zhang, C., Zhao, X., & Xu, X. (2022). Recovery of emulsifying and gelling protein from waste chicken exudate by using a sustainable pH-shifting treatment. *Food Chemistry, 387*, Article 132886. https://doi.org/10.1016/j.foodchem.2022.132886

Kato, A. (2002). Industrial applications of maillard-type protein-polysaccharide conjugates. *Food Science and Technology Research, 8*(3), 193–199. https://doi.org/10.3136/fstr.8.193

Ki, D., Parameswaran, P., Popat, S. C., Rittmann, B. E., & Torres, C. I. (2015). Effects of pre-fermentation and pulsed-electric-field treatment of primary sludge in microbial electrochemical cells. *Bioresource Technology, 195*, 83–88. https://doi.org/10.1016/j.biortech.2015.06.128

Lavelli, V., & Beccalli, M. P. (2022). Cheese whey recycling in the perspective of the circular economy: Modeling processes and the supply chain to design the involvement of the small and medium enterprises. *Trends in Food Science & Technology, 126*, 86–98. https://doi.org/10.1016/j.tifs.2022.06.013

Li, D., Zhao, Y., Wang, X., Tang, H., Wu, N., Wu, F., Yu, D., & Elfalleh, W. (2020). Effects of (+)-catechin on a rice bran protein oil-in-water emulsion: Droplet size, zeta-potential, emulsifying properties, and rheological behavior. *Food Hydrocolloids, 98*, Article 105306. https://doi.org/10.1016/j.foodhyd.2019.105306

Li, Y., Xu, Y., & Xu, X. (2022). Continuous cyclic wet heating glycation to prepare myofibrillar protein-glucose conjugates: a study on the structures, solubility and emulsifying properties. *Food Chemistry, 388*, Article 133035. https://doi.org/10.1016/j.foodchem.2022.133035

Liang, H.-N., & Tang, C.-H. (2013). pH-dependent emulsifying properties of pea [Pisum sativum (L.)] proteins. *Food Hydrocolloids, 33*(2), 309–319. https://doi.org/10.1016/j.foodhyd.2013.04.005

Liu, W., Zhang, H. X., Wu, Z. L., Wang, Y. J., & Wang, L. J. (2013). Recovery of isoflavone aglycones from soy whey wastewater using foam fractionation and acidic hydrolysis. *Journal of Agricultural and Food Chemistry, 61*(30), 7366–7372. https://doi.org/10.1021/jf401693m

Man, H., Jia, Y., Song, H., Yan, X., Zhang, D., Huang, Y., Qi, B., Zhang, S., & Li, Y. (2023). Effects of κ-carrageenan addition and chlorogenic acid covalent crosslinking on protein conformation and gelling properties of soy protein hydrogels. *LWT, 174*, Article 114434. https://doi.org/10.1016/j.lwt.2023.114434

Mohammadian, M., & Madadlou, A. (2016). Characterization of fibrillated antioxidant whey protein hydrolysate and comparison with fibrillated protein solution. *Food Hydrocolloids, 52*, 221–230. https://doi.org/10.1016/j.foodhyd.2015.06.022

Mounsey, J. S., O'Kennedy, B. T., Fenelon, M. A., & Brodkorb, A. (2008). The effect of heating on β-lactoglobulin–chitosan mixtures as influenced by pH and ionic strength. *Food Hydrocolloids, 22*(1), 65–73. https://doi.org/10.1016/j.foodhyd.2007.04.006

Mu, H., Song, Z., Wang, X., Wang, D., Zheng, X., & Li, X. (2022). Microencapsulation of algae oil by complex coacervation of chitosan and modified starch: Characterization and oxidative stability. *International Journal of Biological Macromolecules, 194*, 66–73. https://doi.org/10.1016/j.ijbiomac.2021.11.168

Nguyen, T. T., Luo, X., Su, P., Balakrishnan, B., & Zhang, W. (2020). Highly efficient recovery of nutritional proteins from Australian Rock Lobster heads (Jasus edwardsii) by integrating ultrasonic extraction and chitosan co-precipitation. *Innovative Food Science & Emerging Technologies, 60*, Article 102308. https://doi.org/10.1016/j.ifset.2020.102308

Rabelo, R. S., Tavares, G. M., Prata, A. S., & Hubinger, M. D. (2019). Complexation of chitosan with gum Arabic, sodium alginate and κ-carrageenan: Effects of pH, polymer ratio and salt concentration. *Carbohydrate Polymers, 223*, Article 115120. https://doi.org/10.1016/j.carbpol.2019.115120

Sliwinski, E. L., Roubos, P. J., Zoet, F. D., van Boekel, M. A. J. S., & Wouters, J. T. M. (2003). Effects of heat on physicochemical properties of whey protein-stabilised emulsions. *Colloids and Surfaces B: Biointerfaces, 31*(1), 231–242. https://doi.org/10.1016/S0927-7765(03)00143-7

Song, H., Zhong, M., Sun, Y., Li, Y., & Qi, B. (2023). Recovery of proteins from soybean oil-body wastewater at various pH levels and their structural and functional characterization. *LWT, 174*, Article 114455. https://doi.org/10.1016/j.lwt.2023.114455

Sorgentini, D. A., & Wagner, J. R. (1999). Comparative study of structural characteristics and thermal behavior of whey and isolate soybean proteins. *Journal of Food Biochemistry, 23*(5), 489–507. https://doi.org/10.1111/j.1745-4514.1999.tb00033.x

Tu, C., Azi, F., Huang, J., Xu, X., Xing, G., & Dong, M. (2019). Quality and metagenomic evaluation of a novel functional beverage produced from soy whey using water kefir grains. *LWT, 113*, Article 108258. https://doi.org/10.1016/j.lwt.2019.108258

Vuillemin, M. E., Michaux, F., Muniglia, L., Linder, M., & Jasniewski, J. (2019). Gum arabic and chitosan self-assembly: Thermodynamic and mechanism aspects. *Food Hydrocolloids, 96*, 463–474. https://doi.org/10.1016/j.foodhyd.2019.05.048

Wang, L., Wu, Z., Zhao, B., Liu, W., & Gao, Y. (2013). Enhancing the adsorption of the proteins in the soy whey wastewater using foam separation column fitted with internal baffles. *Journal of Food Engineering, 119*(2), 377–384. https://doi.org/10.1016/j.jfoodeng.2013.06.004

Wang, T., Wang, N., Dai, Y., Yu, D., & Cheng, J. (2023). Interfacial adsorption properties, rheological properties and oxidation kinetics of oleogel-in-water emulsion stabilized by hemp seed protein. *Food Hydrocolloids, 137*, Article 108402. https://doi.org/10.1016/j.foodhyd.2022.108402

Wang, X., Li, X., Xu, D., Zhu, Y., Cao, Y., Wang, J., & Sun, B. (2019). Comparision of heteroaggregation, layer-by-layer and directly mixing techniques on the physical properties and in vitro digestion of emulsions. *Food Hydrocolloids, 95*, 228–237. https://doi.org/10.1016/j.foodhyd.2019.04.034

Wang, Y.-R., Yang, Q., Du, Y.-N., & Chen, H.-Q. (2023). Chitosan can improve the storage stability of ovalbumin fibrils at pH higher than isoelectric point. *Food Hydrocolloids, 136*, Article 108286. https://doi.org/10.1016/j.foodhyd.2022.108286

Wibowo, S., Velazquez, G., Savant, V., & Torres, J. A. (2005). Surimi wash water treatment for protein recovery: Effect of chitosan–alginate complex concentration and treatment time on protein adsorption. *Bioresource Technology, 96*(6), 665–671. https://doi.org/10.1016/j.biortech.2004.06.024

Xie, H., Ouyang, K., Shi, W., Wang, W., Wang, Y., Xiong, H., & Zhao, Q. (2023). Enhancing the interfacial stability of O/W emulsion by adjusting interactions of chitosan and rice protein hydrolysate. *Food Hydrocolloids, 137*, Article 108406. https://doi.org/10.1016/j.foodhyd.2022.108406

Xue, H., Liu, H., Wu, N., Zhang, G., Tu, Y., & Zhao, Y. (2022). Improving the gel properties of duck egg white by synergetic phosphorylation/ultrasound: Gel properties, crystalline structures, and protein structure. *Ultrasonics Sonochemistry, 89*, Article 106149. https://doi.org/10.1016/j.ultsonch.2022.106149

Zhan, F., Shi, M., Wang, Y., Li, B., & Chen, Y. (2019). Effect of freeze-drying on interaction and functional properties of pea protein isolate/soy soluble polysaccharides complexes. *Journal of Molecular Liquids, 285*, 658–667. https://doi.org/10.1016/j.molliq.2019.04.126

Zhang, Q., Dong, H., Gao, J., Chen, L., & Vasanthan, T. (2020). Field pea protein isolate/chitosan complex coacervates: Formation and characterization. *Carbohydrate Polymers, 250*, Article 116925. https://doi.org/10.1016/j.carbpol.2020.116925